

Numerical and experimental investigation of impact on bilayer aluminum-rubber composite plate

Amin Khodadadi¹, Gholamhossein Liaghat^{1,2*}, Davoud Shahgholian-Ghahfarokhi¹,
Mahmoud Chizari³, Bin Wang⁴

¹Department of Mechanical Engineering, Tarbiat Modares University, Tehran, Iran

²Department of Mechanical Engineering, Kingston University, London, United Kingdom

³School of Engineering and Technology, University of Hertfordshire, Hatfield, United Kingdom

⁴Department Mechanical and Aerospace Engineering, University of Brunel, London, United Kingdom

* Corresponding author, Ghlia530@modares.ac.ir and G.Liaghat@kingston.ac.uk

Abstract

This paper aims to investigate the performance of an aluminum–rubber composite plate under impact loading. The impact resistance of the plate has been evaluated using both experimental and numerical methods. The experimental tests were carried out using gas gun at velocities of 75, 101, 144 and 168 m/s. The energy absorption of composite plates has been closely examined for all samples. The effect of rubber layer positioning either on front face or on back face of the aluminum plate was also evaluated. It was found that the composite plate with rubber on front face provides higher performance to absorb the energy. In parallel to the experiment, a finite element model was created using the finite element software LS-DYNA to simulate the response of the aluminum–rubber composite plate under a high energy rate loading condition. The data obtained from finite element modeling shown a close agreement with the experimental results in terms of failure mechanism and energy absorption. In addition, a parametric study was carried out incorporating different impact velocities, rubber formulation, rubber layer thickness, interface bonding strength between rubber and aluminum layers and ballistic performance of aluminum-rubber sandwich panel. It was concluded that by increasing the rubber layer’s thickness the energy absorption of the composite plate will be increased, especially when rubber layer placed in front face of the aluminum plate. Although at high interface bonding of rubber and aluminum layer, the composite with rubber layer in front face has better performance, but low bonding of interface lead to higher energy absorption in back face configuration.

Keywords: Impact loading; Numerical simulation; LS-DYNA; Energy absorption; Bilayer aluminum-rubber composite.

1. Introduction

The protection capability of armor plates made of strong aluminum alloys has been a topic of interest for many years due to their low density, reasonable formability and high impact strength. Many publications deal with the ballistic performance of aluminum plates under impact of projectile through experimental and numerical analysis [1-5].

In recent years, researchers have made significant efforts to improve the performance of metallic structural protections against impact threats [6-8]. One major development has been the use of elastomeric coatings on hard substrates to decrease the damages of blast load and penetration of projectiles. Elastomers can be used to dissipate kinetic energy associated with impacts and shocks. Due to ability of absorption of considerable amount of energy before failure elastomers have been considered as a protective coating for structural and composite system under dynamic loading induced by blast, ballistic and other impact events. Several elastomers have been shown promising results in these applications. Amini et al. [9, 10] investigated the response of monolithic steel plates and steel-polyurea bilayer plates subjected to impulsive and direct pressure pulse. The research was carried out experimentally and numerically, focusing on the deformation and failure modes of the plates. Their results suggested that the polyurea layer can have a significant effect on the response of the steel plate onto dynamic impulsive loads. They have considered the failure mitigation and energy absorption of the plate, if the layer attached on the back face of the plate. Roland et al. [11, 12] reported the ability of polyurea coatings to increase the impact resistance of high hardness steel plates, where they observed the effect of different layer configurations on the residual velocity. They showed that when polyurea applied to the strike face of steel plates provides a significant enhancement in the ballistic resistance of these plates. They have concluded that the most possible reason for this

improvement against impact resistance of the polyurea-coated steel is a phase transition of the polyurea from the rubbery phase to the glassy phase. This hypothesis was supported by Grujicic [13] using a computational model to evaluate the energy absorption when a deformation-induced glass transition occurs.

Natural rubber (NR) is an appropriate material which can be used as a layer on a rigid substrate. Rubber materials have been widely used in shock absorbers, impact resistance panels and other engineering applications [14, 15]. High level of damping property [16], high level of flexibility [17], and excellent puncture and tear resistance [18] are the specific properties of NR. These features make NR a good candidate to be used as reinforcement in a composite structure [19-22]. To convert a raw NR into a material with desired properties, some ingredients such as fillers, activators, sulfur or other equivalent curatives and accelerators should be added to the raw NR. Variation of compound ingredients alters the mechanical properties of rubber [23]. These additives modify the rubber by forming cross-links between polymer chains. One of the most important ingredients is filler including carbon black and calcium carbonate [24-26]. These fillers are added to rubber formulation to improve the mechanical properties of NR.

As highlighted above, although there are some researchers who investigated the impact response of metallic plates coated by polyuria elastomer but impact response of bilayer aluminum-rubber composite is not investigated yet. Therefore, there is a knowledge gap in this area to understand the effect of the rubber panel on the energy absorption of an aluminum plate. In order to explore the ballistic performance of these composites, experimental studies were conducted using hemispherical projectiles with impact velocities of 75, 101, 144 m/s and 168 m/s. During the experiments, the focus was on the significance of positioning the rubber layer onto the front face or onto the back face of the aluminum plate. Intention was to look for

probable configuration of bilayer aluminum-rubber composite which provides more energy absorption. In parallel, the failure mode of layer was closely monitored and the observation was mimicked to create a computer simulation. The numerical model was then used to carry a series of parametric studies to investigate the parameters which affect the impact resistance of bilayer aluminum-rubber composite.

2. Experimental procedure

2.1. Materials and specimen preparation

Aluminum alloy has been used as a candidate material in many engineering applications due to its low density and high ductility and its reasonable strength. In this study, Aluminum 2024-T3 was used to carry the experimental tests. The stress-strain curve of Aluminum 2024-T3, which was obtained from tensile test, was shown in Fig 1 and its mechanical properties were reported in Table 1.

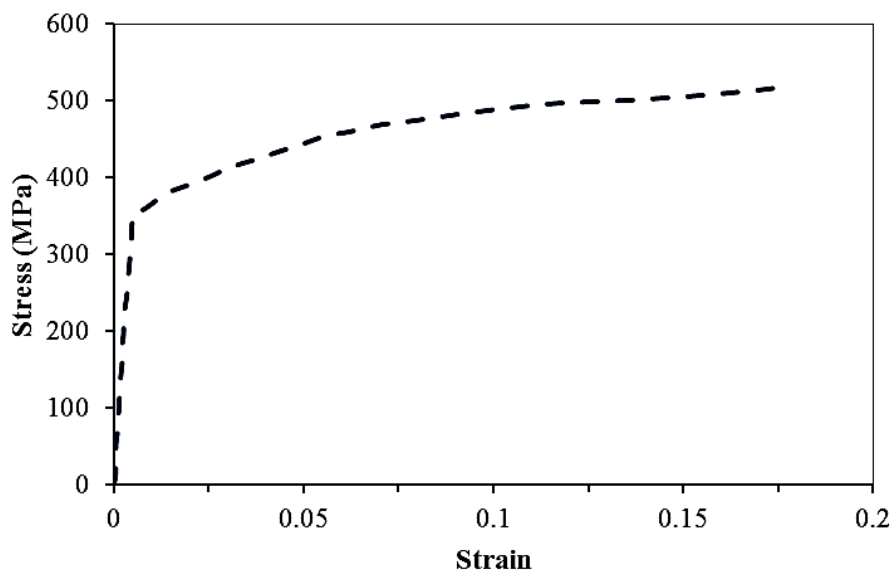


Fig. 1 Tensile stress–strain curve of aluminum 2024-T3

Table 1 Mechanical properties of aluminum 2024-T3

Property	Value
Density, ρ (kg/m ³)	2700
Elastic modulus, E (MPa)	72200
Yield stress, σ_y (MPa)	350
Poisson ratio, ν	0.32
ϵ_f	0.18

Natural rubber (SMR 20) with Mooney viscosity of 65 was used to carry the experiments in this study. The SMR 20 material was supplied by the Rubber Research Institute of Malaysia. Compound ingredients named fillers such as carbon black and calcium carbonate were added to the rubber formulation to improve its mechanical properties. In rubber compound, ZnO, stearic acid, accelerators and sulfur constitute the vulcanization system which is used for crosslinking of the matrix phase. To evaluate the behavior of rubber with different components at high strain rates, two types of rubber with different formulation were used. The NR compounds formulation for two types of compounds with high hardness (HH) and low hardness (LH) is presented in Table 2. Compounding were performed on an open two-roll mixing mill (Polymix 200 L, Germany) and were cured under hydraulic pressure according to the rheometer results which is presented in Fig.2 for both LH and HH rubber.

Table 2 Formulation of the rubber compounds

Ingredients	Loading (Phr)	
	Formulation 1	Formulation 2
NR	100	100
Carbon Black (N330)	60	40
Zink oxide	5	5
Calcium carbonate	30	30
Spindle oil	15	30
Sulfur	2	1.5
Volcacit	0.7	0.7

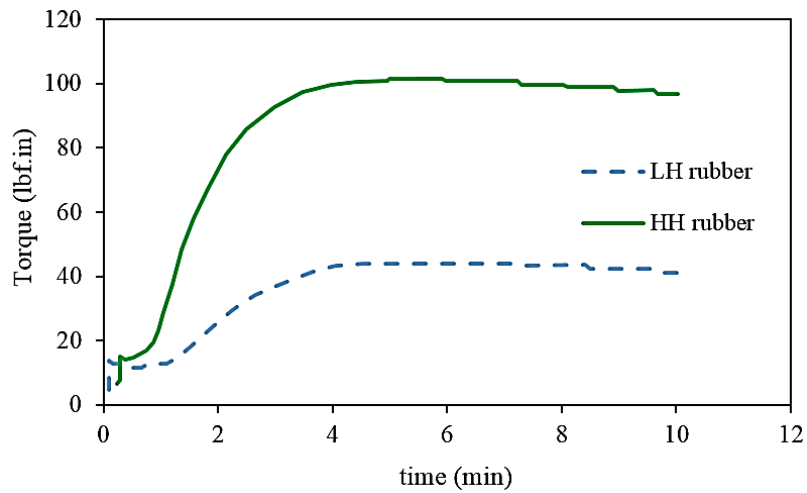


Fig. 2 Rheometer curves

To prepare the specimens, a layer of aluminum with thickness of 0.5 mm and rubber layer with 2 mm were bonded together by BYLAMET S2 adhesive. Before bonding, the aluminum plate was carefully cleaned using acetone. To obtain a strong bonding between aluminum and rubber plates, a pressure was applied on the specimen. Fig. 3 shows the bilayer aluminum-rubber specimen and its dimensions.

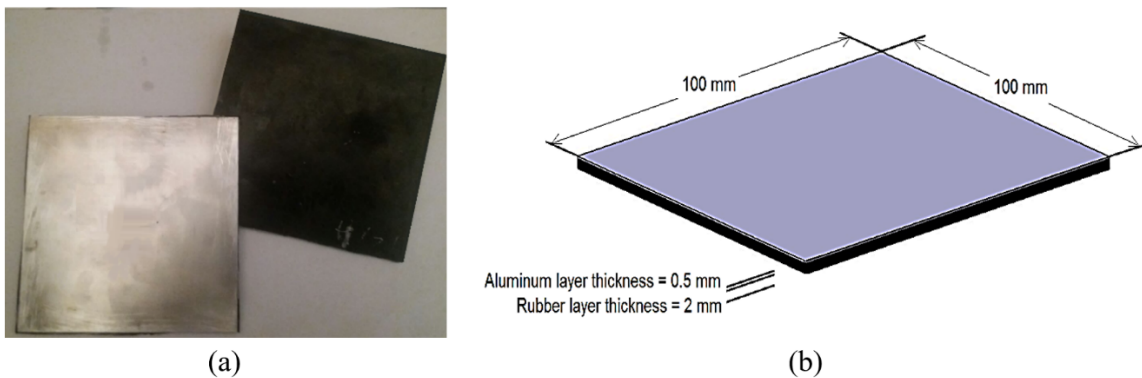


Fig. 3 (a) Aluminum-rubber specimens (b) Dimension of specimens

2.2. Impact tests

Impact tests were performed using a gas gun as shown in Fig. 4. The gas gun was made of a pressure vessel with 120 bar capacity, a high speed firing valve and a hollow steel barrel with 6

m long. The inside diameter of barrel was 10 mm. The exact impact velocity of each projectile was measured with a chronograph (model M-1, Chrony Canada) before and after impacting the target. Fixture for holding the specimens was located in the target chamber. The projectile used for ballistic tests was made of steel and were hardened by heat treatment to minimize projectiles' deformation. The physical properties of projectile were presented in table 3.

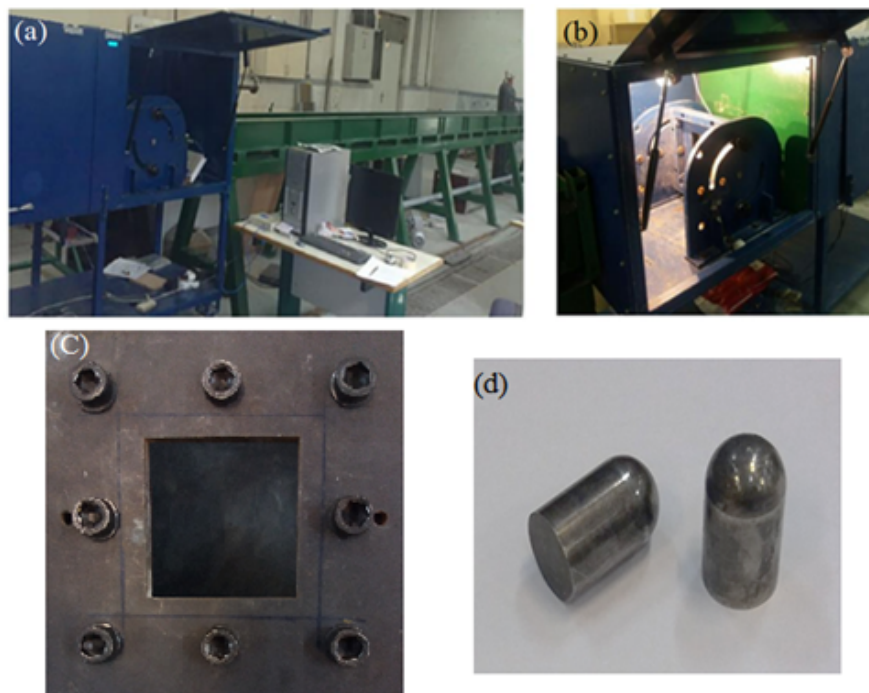


Fig. 4 (a) Gas gun (b) Target chamber (c) Fixture (d) Projectiles

Table 3 Physical properties of projectile

Length (mm)	Diameter (mm)	Weight (g)	Hardness (RC)
16.75	10	9.32	55-56

2.3. SHPB experiment

High strain rate tests on the rubber sample were conducted using Split Hopkinson Pressure Bar (SHPB) to obtain the samples stress–strain properties at different strain rates. The conventional steel SHPB helps to test metallic materials, but it cannot precisely determine the dynamic responses

of soft materials like rubber [27]. The tests were performed using nylon bars instead of metal bar owing to this limitation. The mechanical impedance of nylon bars is much closer to that of the rubber specimens. Thus, the transmitted wave is sufficiently large for measurement. The Split Hopkinson Pressure Bar (SHPB) system, striker bar and rubber specimen are presented in Fig. 5. The ratio of optimal length-to-diameter (L/D) in the specimens for the SHPB test is 0.5, which was used to minimize inertia and friction effects [28]. To ensure homogeneous deformation and stress equilibrium during the experiment, the length of soft material specimens must be sufficiently short. In this study, the length of the specimen was designed to be 5 mm.

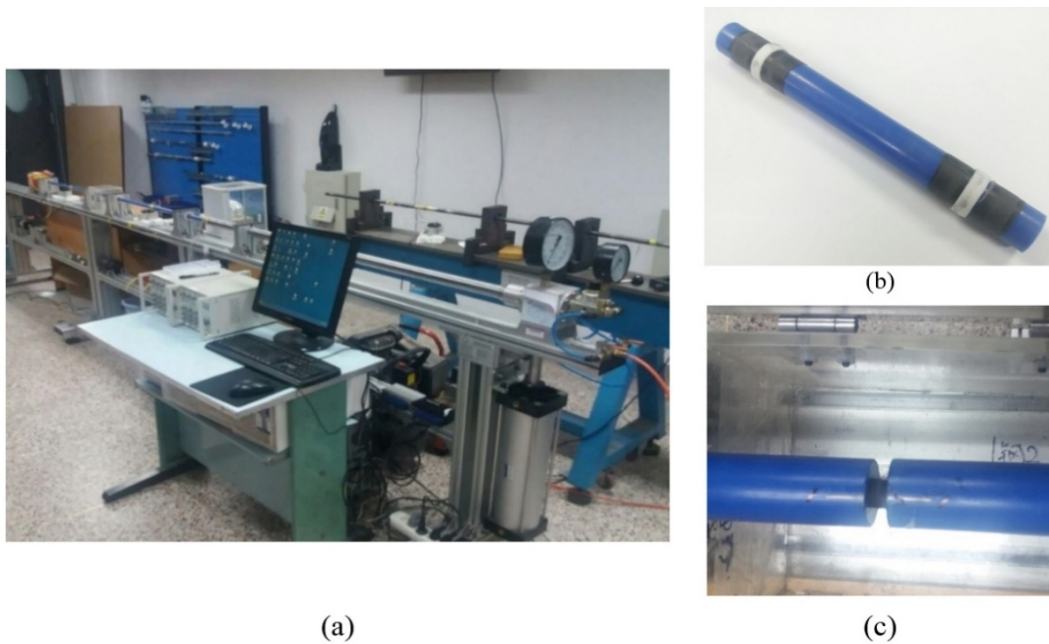


Fig. 5 Split Hopkinson Pressure Bar test (a) SHPB machine (b) Striker bar (c) rubber Specimen.

3. Numerical analysis

3.1. Geometry modelling

The commercial finite element software, LS-DYNA V9.71, was used to simulate the response of aluminum-rubber composite under impact loading. LS-DYNA is a non-linear dynamic modeling software that benefits explicit formulation. The numerical model consists of a

projectile with initial velocity and a bilayer aluminum-rubber composite plate. Fig. 6 shows the finite element model of projectile and target for rubber layer located on the impact face (front face; FF) and second the rubber layer located on the face opposite to the impact side (back face; BF). aluminum-rubber composite was modeled with the dimensions of 100×100 mm. Clamped boundary condition was assigned to the model to restrict all degrees of freedom at edges as shown in Fig. 6(c). To include out-plane stress components, the composite model was meshed with 8-node reduced integration solid element. Mesh sensitivity was checked by varying the number of the elements along the bilayer aluminum-rubber composite thickness to obtain the residual velocity of projectile with adequate accuracy. The mesh of bilayer plate included a total number of 400000 elements. 160000 elements in aluminum layer with the mesh size of 0.5×0.5×0.125 mm and 240000 elements with the mesh size of 0.5×0.5×0.33 mm for rubber layer. Also the projectile’s mesh had 12900 elements.

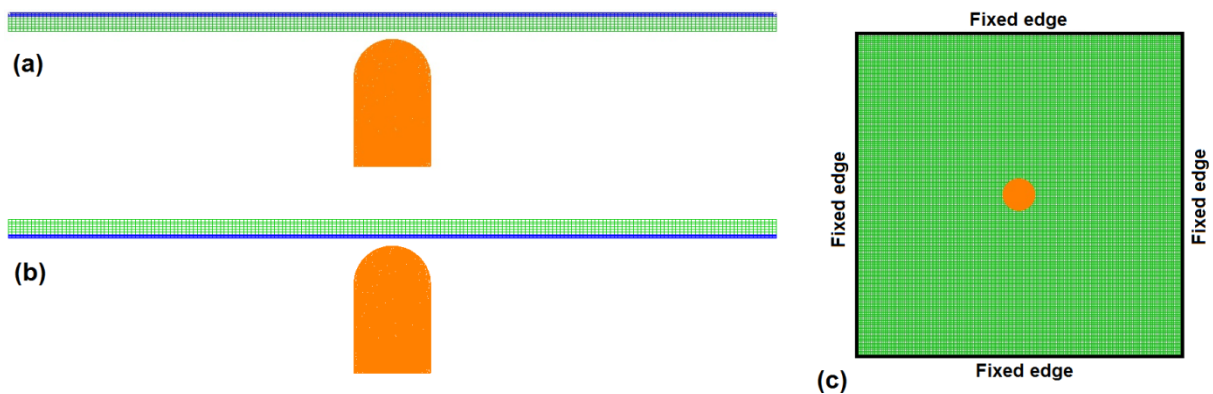


Fig. 6 Finite element model (a) rubber layer located on the impact face (b) rubber layer located on the opposite of the impact face (c) Boundary conditions

3.2. Material modeling

3.2.1. Aluminum plate

Material model 3 in LS-DYNA software (MAT_PLASTIC_KINEMATIC) was chosen to describe elastic–plastic behavior of the aluminum plate. This material model uses an isotropic constitutive based on isotropic and kinematic hardening [29]. Also, strain rate effects are estimated by Cowper–Symonds constitutive relationship.

$$\sigma_{y-dyn} = [1 + (\dot{\epsilon}/C)^{1/P}] (\sigma_{y-st} + E_p \epsilon_p) \quad (1)$$

In Eq. (1), P and C are empirical constants, and for aluminum alloys are 4 and 6500 1/s, respectively [30, 31]. Also, E_p is calculated as shown in Eq. (2).

$$E_p = E E_t / (E - E_t) \quad (2)$$

Where E_t is tangent modulus of bilinear stress–strain curve.

The plastic-kinematic material model which was used with Cowper–Symonds constitutive relationship, is an appropriate to model the failure and fracture of aluminum plate. Fracture strain was considered as criteria to model failure. As the projectile hits the aluminum plate its nose pushes the front surface of it which caused generation of compressive stress at the target surface. Further movement of the projectile created the tensile stretching of the material due to which thinning of the material was observed particularly close to contact region between the target and the projectile. Finally, by exceeding the element strain from fracture strain, the element is deleted from simulation.

3.2.2. Rubber layer

LS-DYNA offers several material models of rubber-like materials. In this research Mooney-Rivlin model has been chosen which the strain energy function is given by:

$$W = C_{10}(I_1 - 3) + C_{01}(I_2 - 3) \quad (3)$$

Where I_1 and I_2 are the principal invariants of the left Cauchy–Green deformation tensor, defined by:

$$\begin{aligned} I_1 &= \text{tr}C = \lambda_1^2 + \lambda_2^2 + \lambda_3^2 \\ I_2 &= \frac{1}{2}[(\text{tr}C)^2 - \text{tr}C^2] = \lambda_1^2 \lambda_2^2 + \lambda_1^2 \lambda_3^2 + \lambda_2^2 \lambda_3^2 \\ I_3 &= \det C = \lambda_1 \lambda_2 \lambda_3 \end{aligned} \quad (4)$$

Where λ_1 , λ_2 and λ_3 are the principal stretches. The Mooney–Rivlin model does not take the strain rate effect into consideration. However, with certain adjustment, the Mooney–Rivlin model can be used in the simulations. Fig. 7 shows the stress–strain curves at different strain rates obtained by SHPB tests for two LH and HH natural rubber. The strain rate that the material undergoes during the penetration process was estimated by impact simulation on pure rubber panel. The study used the strain rate about 4000 s^{-1} for the rubber and fitted it with Mooney–Rivlin material model, using least squares approach. The calibrated coefficients of C_{10} and C_{01} are 5.6 and 0.5, respectively for HH rubber and 2.9 and 0.4 for LH rubber. The maximum principal strain is used as the failure criterion of the rubber. The pure rubber panel was modeled by LS-DYNA and impact response of panel was simulated and verified by the authors' previous experimental work [32]. Although, results of quasi-static test show the HH and LH rubber strain to break are about 2.2 and 3.5 under quasi-static test but from a series of simulations, it was estimated that the fracture strain for the rubber material is 1.20 and 1.70 under high strain rate. Split Hopkinson pressure bar results show that in high strain rates, rubber material behaves stiffer. It can be seen that by increasing the strain rate, the strain-stress curve transfers to higher values, which means higher stiffness. On the other hand, it was shown by Roland [11], when an

elastomer was loaded in high strain rates, its behavior transfers from elasticity to brittle behavior.

This means its elongation capacity decreases and rubber fails at lower strain values.

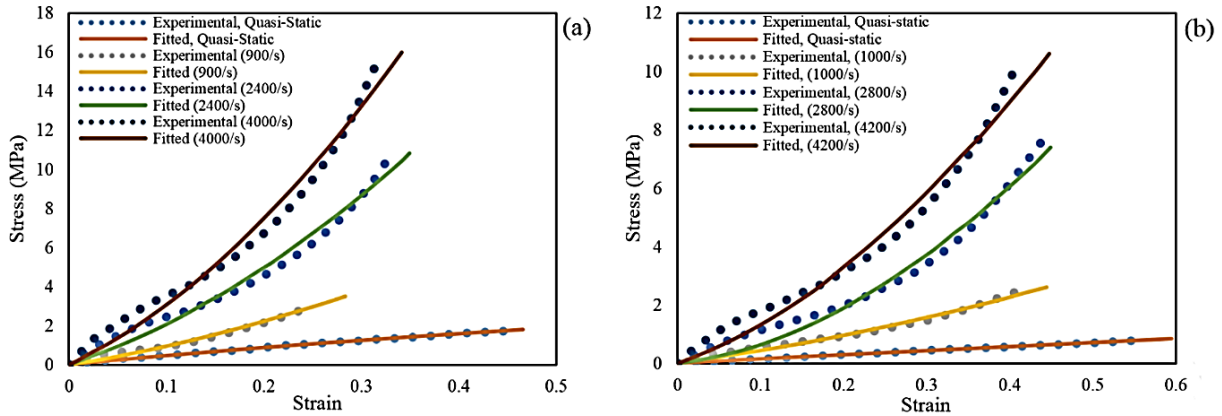


Fig. 7 Stress-Strain curves of rubber at different strain rates (a) high hardness rubber (b) low hardness rubber

3.3. Contact modeling

To allow the removing of elements due to the impact of projectile, CONTACT_ERODING_SURFACE_TO_SURFACE was added between the projectile and target layers. Also results of impact tests on bilayer aluminum-rubber composite indicated that debonding is an important failure mode. This fact led to the necessity to implement debonding in the modelling of composite. Debonding in LS-DYNA was modeled through the TIEBREAK_SURFACE_TO_SURFACE contact algorithm. Tiebreak is active for nodes which are initially in contact. This contact algorithm incorporates failure criteria that, when achieved, release the tied interface between the contacting faces and the constraint is transformed to surface-to-surface contact that allows sliding between the faces while preventing the penetration of nodes between the parts in contacts. Debonding occurs when the following equation is satisfied:

$$\left(\frac{\sigma}{NFLS}\right)^2 + \left(\frac{\tau}{SFLS}\right)^2 \geq 1 \quad (5)$$

Where σ and τ are the normal and shear stresses at the interface, and SFLS and NFLS are the interface normal and shearing strengths. Because there was no any bonding strength experimental data at the time, a trial and error method was employed to reproduce the experimentally observed debonding by adjusting the value of the interface bonding strength. In a final simulation, the SFLS and NFLS were taken to be 80 MPa and 50 MPa, respectively. Debonding of composite obtained experimentally and numerically for two BF and FF configurations are shown in Figs. 8 and 9. The comparison of the experimental results and the numerical predictions, shows that the estimated data for bonding strength values are accurate enough to predict the debonding of composite layers under impact loading.

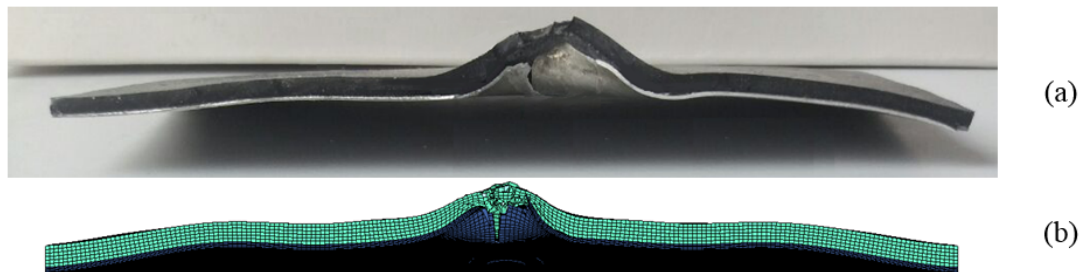


Fig. 8 Comparison of (a) experimental and (b) numerical results with the rubber on the back face at the impact velocity of 144 m/s

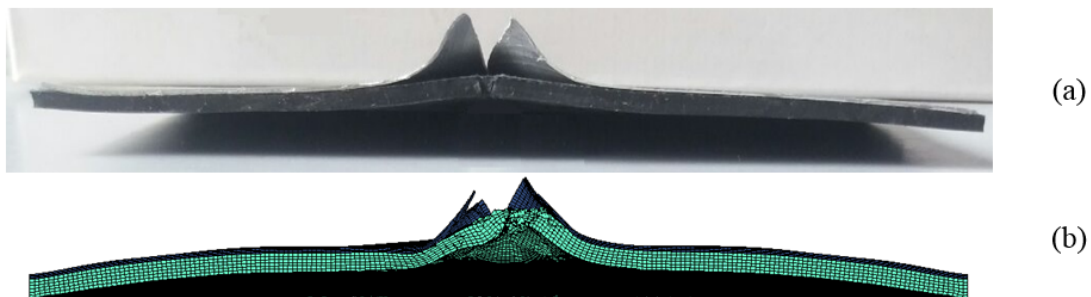


Fig. 9 Comparison of (a) experimental and (b) numerical results with the rubber on the front face at the impact velocity of 144 m/s

4. Results and discussion

The main objective of this study is to investigate the behavior and impact resistance of aluminum-rubber composite plate. The effect of rubber layer on energy absorption and failure mechanism of the composite plate has been studied. To carry on the study a series of experimental tests and numerical analysis were performed on single layer aluminum plate and bilayer aluminum-rubber samples.

4.1. Impact on aluminum plate

To evaluate the impact resistance of aluminum plate, impact tests were conducted using gas gun at five different gas reservoir pressure of 6, 9, 12, 15 and 18 bar. These pressure launched the projectile with the velocities of 75, 96, 109, 122 and 129 m/s respectively. These values were chosen to be greater than ballistic limit. The hemispherical projectile impacted the 0.5 mm aluminum plate and residual velocity, global deformation and the fracture mechanisms were evaluated. The score of the impact on the plate at penetration zone, had 4 petals. By increasing the impact velocity, the larger petals were shown at penetration zone.

A numerical simulation was performed to investigate the aluminum plate behavior under impact loading. This was done in parallel with the experiment to validate the energy absorption of the target plate at velocities which experiments were performed. The failure mode also was compared with the experiments. Fig. 10 shows the perforated aluminum plate at incidence velocity of 109 m/s. Four petals formed at this velocity have been compared experimentally and numerically in Fig. 10a-b. The compared results show, the predicted numerical model is in close agreement with the experiment. Plate was deformed under impact of projectile and when the stress is beyond the tensile strength of material, cracks appear in vicinity of the impact zone.

Cracks will be propagated until the projectile perforates the plate. The perforation process is shown in Fig. 11.

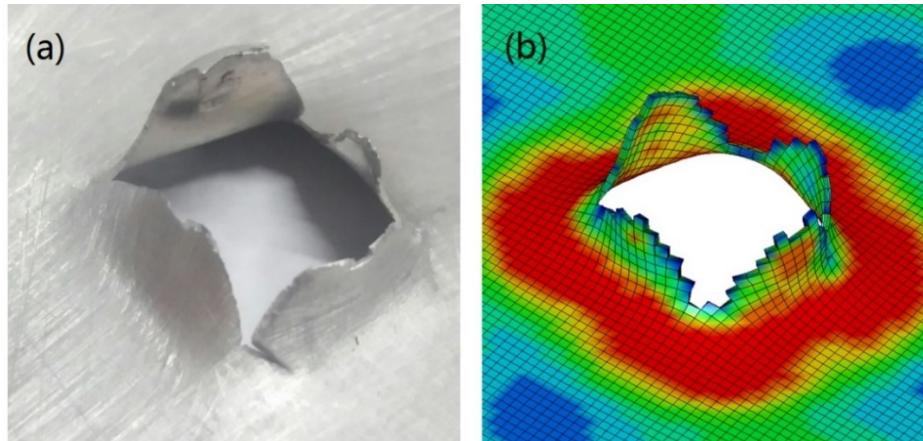


Fig. 10 Comparison of (a) experimental and (b) numerical results at initial velocity of 109 m/s.

The projectile's residual velocity versus impact initial velocity of the aluminum plate is shown in Fig. 12. The residual velocities from the simulations show good agreement with the experimental test results. To determine the ballistic limit velocity, simulation was carried out considering different velocities. The aim was to find a velocity in which the residual velocity becomes zero when the projectile was completely perforated into the specimen. The ballistic limit velocity of monolithic aluminum plate was found to be 50.5 m/s.

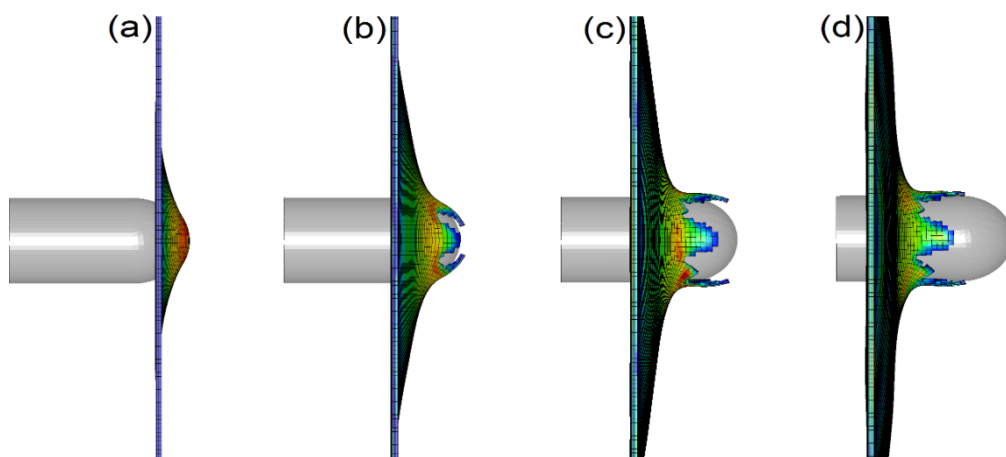


Fig. 11 Perforation of projectile at initial velocity of 129 m/s at (a) 30 (b) 60 (c) 90 and (d) 120 μ s time interval.

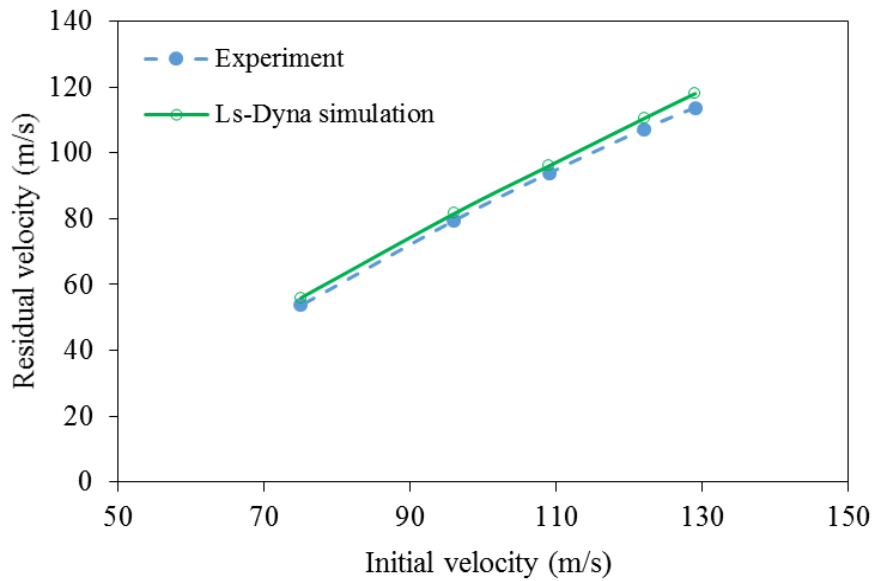


Fig. 12 Experimental and numerical comparison of residual velocity versus impact velocity after perforating the aluminum plate

4.2. Impact on aluminum-rubber plate

The aluminum-rubber bilayer samples were setup using two different configurations: first the rubber located on the impact face (front face; FF) and second the rubber layer located on the face opposite to the impact side (back face; BF). Tests were conducted at four different velocity groups of 75 m/s, 101 m/s, 144 m/s and 168 m/s. Each test repeated five times and average velocity was calculated for each test group.

The experimental and numerical behavior of the aluminum-rubber composite when rubber layer located on the back face (BF) are presented in Figs. 13-15 under the impact velocities of 75 m/s, 144 m/s and 168 m/s, respectively. A good agreement is shown between numerical and experimental results. The damage occurred in case of 75 m/s which is lower than ballistic limit velocity is shown in Fig. 13. In this case, Aluminum layer was damaged and projectile penetrated the aluminum layer, but rubber panel resisted against projectile impact. Also projectile rotation was observed when impact velocity is lower than ballistic limit velocity. In

impact velocities higher than ballistic limit (Figs. 14 and 15), projectile perforated the bilayer composite and passed the target without rotation.

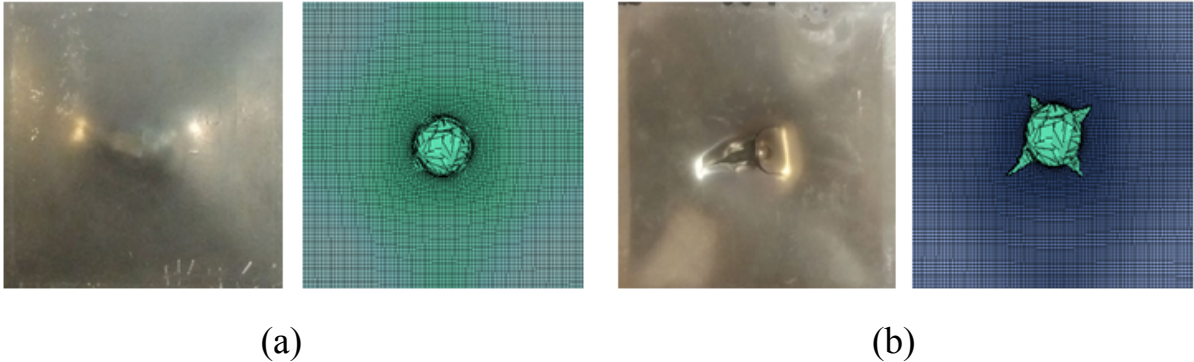


Fig. 13 Failure of composite with the rubber on the back face at the impact velocity of 75 m/s obtained Experimentally and numerically (a) Back view (b) Front view

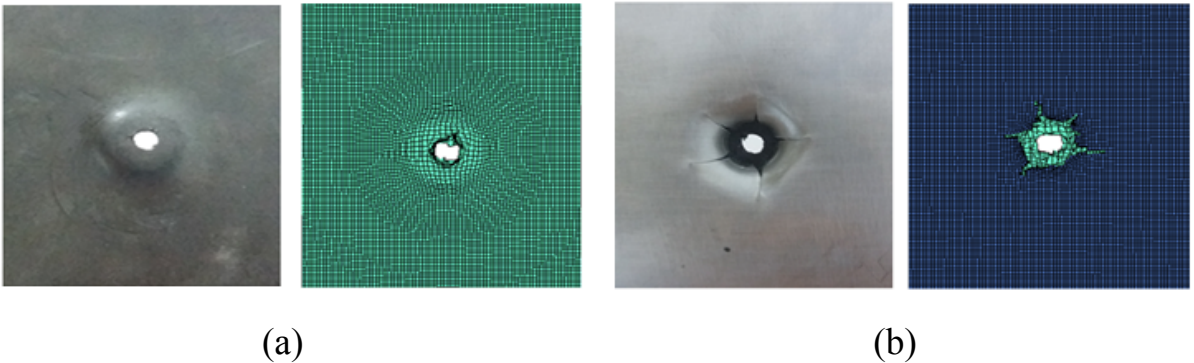


Fig. 14 Failure of composite with the rubber on the back face at the impact velocity of 144 m/s obtained Experimentally and numerically (a) Back view (b) Front view

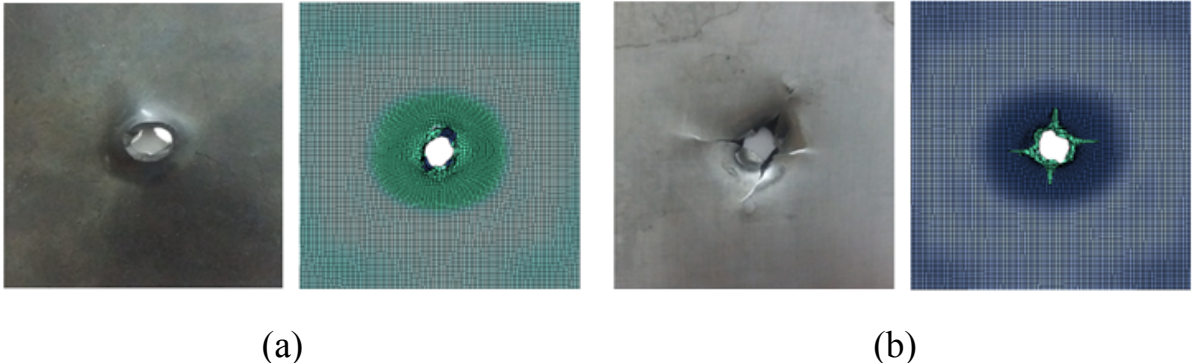
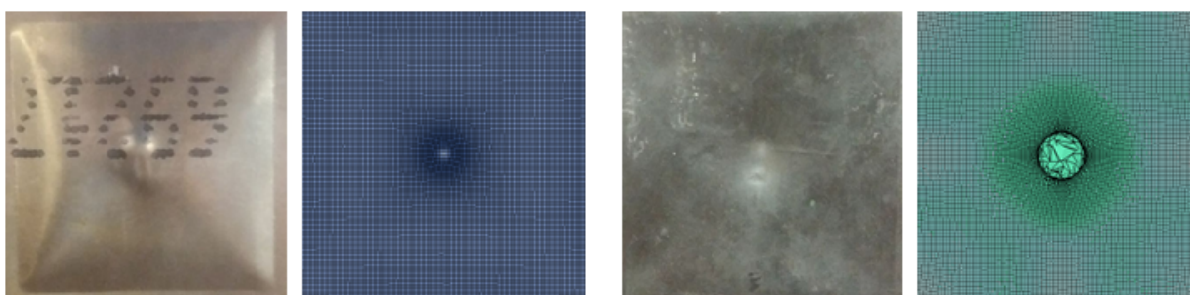


Fig. 15 Failure of composite with the rubber on the back face at the impact velocity of 168 m/s obtained Experimentally and numerically (a) Back view (b) Front view

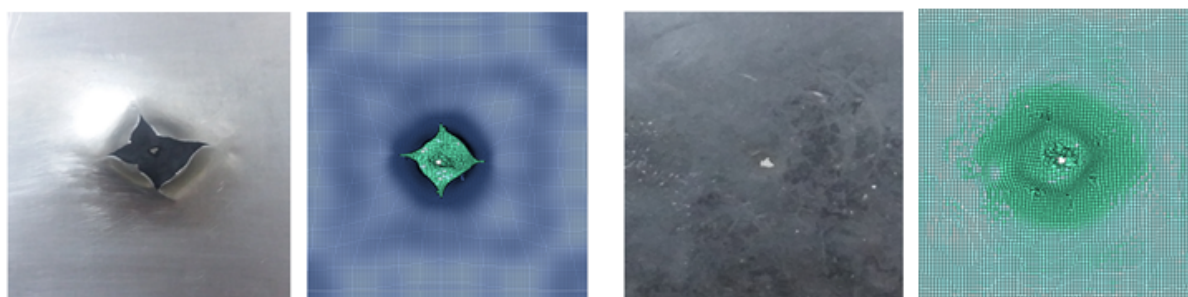
Response of the composite plate when the rubber layer is located on the front face (FF) under the similar impact velocities are shown in Figs. 16-18. It is shown that in this configuration, model predictions are in good agreement with experimental results. The response of bilayer composite when projectile velocity is lower than ballistic limit velocity is shown in Fig. 16. In this case, aluminum layer was deformed but no damage and fracture was observed in composite. Similar to BF configuration, projectile rotation was observed when impact velocity is lower than ballistic limit velocity. Also in impact velocities higher than ballistic limit (Figs. 17 and 18), projectile perforated the bilayer composite and passed the target without rotation.



(a)

(b)

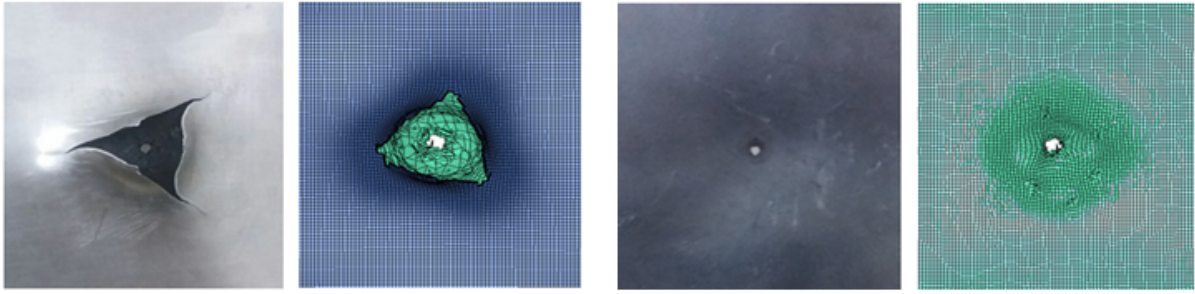
Fig. 16 Failure of composite with the rubber on the front face at the impact velocity of 75 m/s obtained Experimentally and numerically (a) Back view (b) Front view



(a)

(b)

Fig. 17 Failure of composite with the rubber on the front face at the impact velocity of 144 m/s obtained Experimentally and numerically (a) Back view (b) Front view



(a)

(b)

Fig. 18 Failure of composite with the rubber on the front face at the impact velocity of 168 m/s obtained Experimentally and numerically (a) Back view (b) Front view

It was assumed that the loss of projectile's kinetic energy is equal to the energy absorption performed by the composite target in at the perforation event. Therefore the energy absorption of the composite target can be theoretically calculated by subtracting the residual energy of the projectile from its initial energy as presented below.

$$E_p = \frac{1}{2} m_p (V_i^2 - V_r^2) \quad (6)$$

Where E_p (J) is dissipated energy during the impact process, m_p (kg) is mass of the projectile, V_i (m/s) is projectile initial velocity, and V_r (m/s) is residual velocity. Table 4 presents the experimental and numerical results performed for BF and FF configurations. In this table, the experimental test results, which were performed at velocities of 75, 101, 144 and 168 m/s, are presented. A high hardness rubber layer was used for experimental tests. The residual velocity of the projectile was measured and the energy absorption is determined using Equation (6). Energy absorption is used as criteria to evaluate the ballistic performance of the composite plate. Table 4 indicates that the numerical model can be used to estimate the projectile residual velocity and energy absorbed by bilayer composite.

Table 4 Comparison of energy absorption obtained by experimental and numerical simulation

Configuration	Impact velocity (m/s)	Experimental residual velocity (m/s)	Numerical residual velocity (m/s)	Experimental energy absorption (J)	Numerical energy absorption (J)	Error (%)
Rubber in back face	75	0	0	26.2	26.2	0
	101	58.4	64.5	31.6	28.1	11.1
	144	114.6	117.2	35.4	32.6	7.9
	168	138.7	141.5	41.9	38.2	8.8
Rubber in front face	75	0	0	26.2	26.2	0
	101	44.8	53.6	38.2	34.1	10.7
	144	104.5	107	45.7	43.3	5.2
	168	133.9	137.6	48	43.3	9.8

5. Parametric study

A parametric study on bilayer aluminum-rubber composite plate under impact loading was performed. The main parameters that were investigated are: the relative position of the rubber layer with respect to the loading direction, the effect of different impact velocities, the effect of rubber hardness, the effect of rubber layer thickness, the strength of rubber-aluminum bonding and ballistic performance of aluminum-rubber sandwich panel. The residual velocity of projectile was measured in simulations and the energy absorption of bilayer composite was calculated and considered as a criterion to compare their impact resistance. The projectile used in the finite element models reported in this section has a mass of 9.32 g for all the modeled samples. Also, all the aluminum plate models have thickness of 0.5 mm.

5.1. Effect of relative position

As it is mentioned in the previous section, to study the effect of the relative position of rubber, two configurations of bilayer composite plate were considered. First configuration, the rubber

layer was located on the impact receiving side, front face (FF), and second, the rubber panel was located on the back face of impact (BF). In this section numerical simulation was performed in different impact velocities to see the effect of rubber layer position. Also, the ballistic limit of the composite target was determined. The high hardness (HH) rubber layer was used and the interface shear and normal bonding strength was assumed to be 80 and 50 MPa, respectively. Rubber layer with thickness of 2 mm and aluminum layer with thickness of 0.5 mm were used to investigate the effect of relative position. Figure 19 shows the residual velocity of projectile after perforating the bilayer composite versus impact velocity for two BF and FF configurations. Moderate enhancement in ballistic performance in terms of lower residual velocity for bilayer composite plate, which rubber layer located in front face, was observed and compared to the corresponding back face configuration. It was find out that the composite plate by front face rubber layer configuration shows a better penetration resistance compared to the back face composite plate.

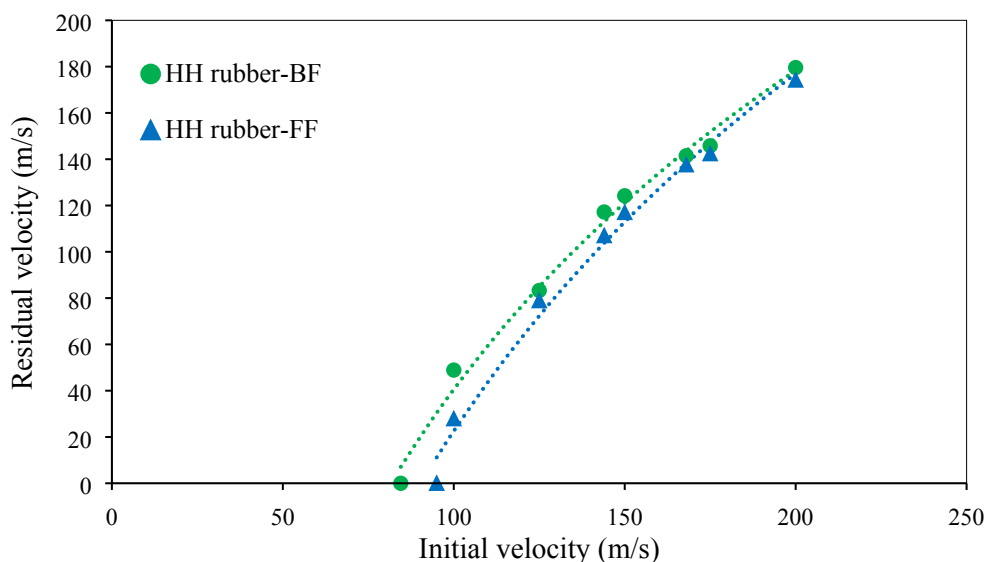


Fig. 19 Residual velocities versus initial velocities of Al-HH rubber composite for BF and FF configuration

The ballistic limits obtained by numerical analysis for the composite plate with BF and FF configurations are 84.5 and 95 m/s, respectively. While, in Section 4.1, it was observed that the ballistic limit for the single-layer aluminum plate is 50.5 m/s. Comparing the ballistic limit of the bilayer aluminum-rubber composite with the ballistic limit of the aluminum plate shows the rubber layer with high damping properties has a significant effect on the energy absorption of the composite target. Increase in the ballistic limit of composite with the BF and FF configurations is 67.3% and 88.1%, respectively.

5.2. Effect of rubber hardness

It is known that in rubber material the formulation of its component has influence on its mechanical properties and its impact resistance properties. In this section the numerical simulation was performed on the bilayer aluminum-low hardness rubber (LH) composite plate and compared to the composite plate made by HH rubber. Rubber layer with thickness of 2 mm for both LH and HH rubber and aluminum layer with thickness of 0.5 mm were used to investigate the effect of rubber hardness. Figs. 20 and 21 show the residual velocity of projectile versus initial velocity after perforation of two types composite with HH and LH rubber layer for BF and FF configuration. The figures show higher ballistic performance in term of lower residual velocity for the composite plate made by HH rubber compared to corresponding LH rubber composite plate. This advantage is applicable for both BF and FF configurations. The higher energy absorption capacity of HH rubber compare to LH rubber can be referred to its stronger molecular chains.

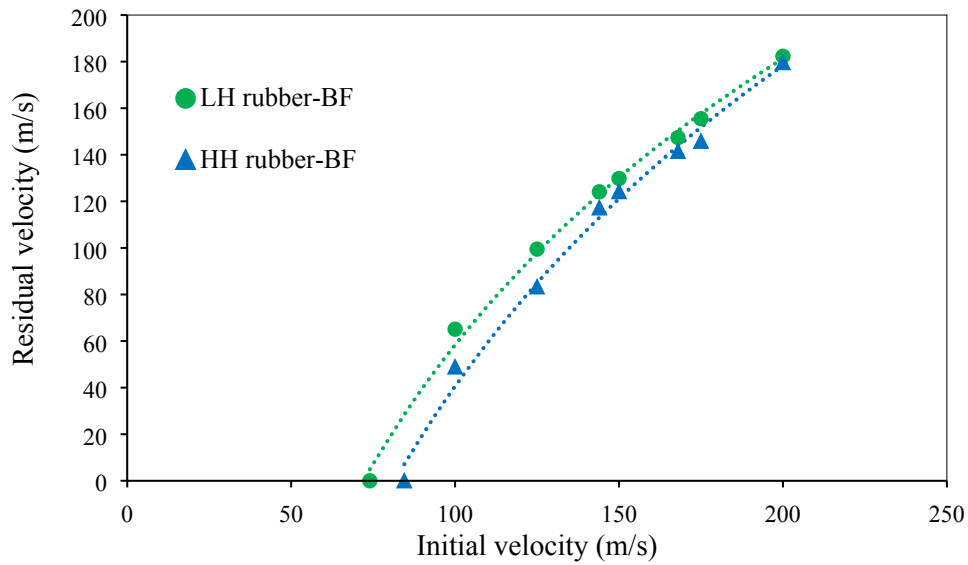


Fig. 20 Residual velocities versus initial velocities of Al-rubber composite with LH and HH rubber layer for BF configuration

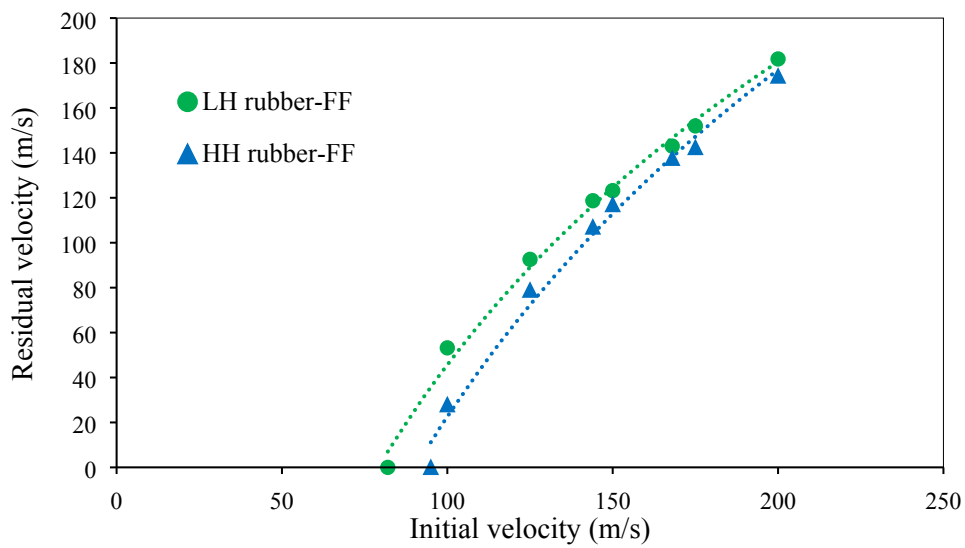


Fig. 21 Residual velocities versus initial velocities of Al-rubber composite with LH and HH rubber layer for FF configuration

Fig. 22 illustrates the projectile velocity histories at impact velocity of 150 m/s on the bilayer composites plate made by LH and HH rubber layers for BF and FF configurations. As it is shown in the figure, the specimens' perforation and the residual velocities are different. From observations of Figure 22, following points are notable:

(i) The velocity deceleration rate of the projectile impacting the composite target with HH rubber is higher than the LH case, which means the deceleration rate of the composite sample is directly related to the hardness of the rubber.

(ii) The residual velocity of the projectile impacting the aluminum-HH rubber layer is lower than the aluminum-LH rubber composite sample.

(iii) The first level of composite behavior with BF configuration is affected by the aluminum performance causing the intense deceleration of the projectile velocity. After failure of the aluminum plate, the gradient is gentle due to low module and large elongation to failure of the rubber.

(iv) Time duration of penetration is longer for the composites targets with FF configuration compared with the composites targets with BF configuration.

(v) The residual velocity of the projectile impacting on the composite plate with FF configuration is lower compared to BF configuration.

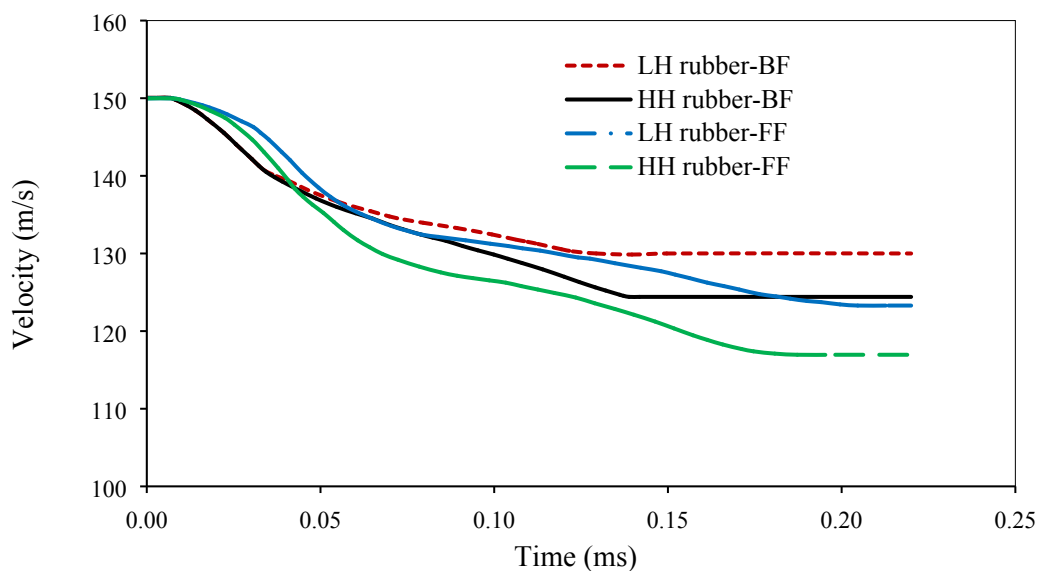








Fig. 22 Comparison of projectile velocity histories at impact velocity of 150 m/s on LH and HH Al-rubber composite for BF and FF configuration

5.3. Effect of rubber layer thickness

A set of simulations was performed to study the effect of the rubber layer thickness on the performance of the bilayer Al-rubber composite target. In these simulations the thickness of aluminum layer was 0.5 mm and the thicknesses of the rubber layer were 0.5 mm, 1 mm, 1.5 mm, 2 mm, 2.5 mm, and 3 mm, as shown in Table 5. The simulations were performed for both BF and FF configurations. The HH rubber layer was used and the interface shear stress and normal stress at bonding interface was assumed to be 80 MPa and 50 MPa, respectively.

Fig. 23 compares the energy absorption of each composite plate with different rubber layer thickness. The comparison reveals that the increase in the thickness of the rubber layer improves the overall performance of the bilayer plates for both BF and FF configuration. In the case of FF configuration the rubber thickness is more effective, in which increasing the rubber layer thickness, significantly increase the energy absorption of the composite target.

Table 5 Numerical modeling of Al-rubber composite with different rubber thickness

Al thickness (mm)	Rubber thickness (mm)	Al-rubber composite
0.5	0.5	
	1	
	1.5	
	2	
	2.5	
	3	

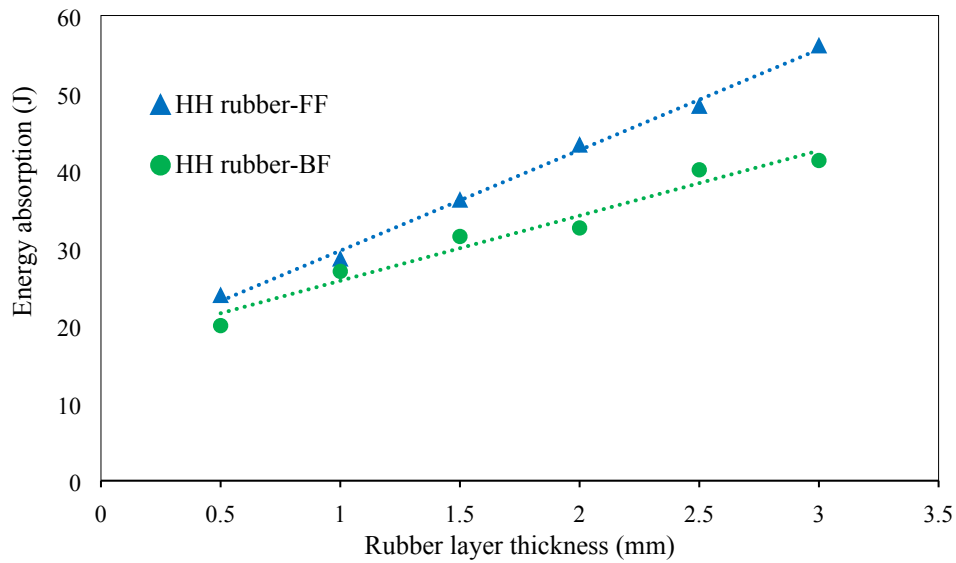


Fig. 23 Energy absorption of Al-HH rubber composite with different rubber layer thickness for BF and FF configuration

5.4. Effect of bonding

A simulation was performed to evaluate the effect of the aluminum-rubber interface bonding strength on the performance of the bilayer composite plate. The thicknesses of aluminum and rubber layer were 0.5 mm and 2 mm, respectively and HH rubber was used in these simulations. The initial velocity of projectile was set to be 144 m/s for each simulation. For all simulation residual velocity was measured and the energy absorption was calculated. The values of the bonding strength used for these simulations are from the low to high bonding values. Six values of interface bonding strength were considered in this study and simulation was performed to evaluate the ballistic performance of each configuration and bonding interface. The bonding values between rubber and aluminum layer were considered to be 0-0 (which means two layers does not have any bonding and are separated with each other), 20S-12N, 40S-25N, 60S-38N, 80S-50N, and Tie (perfect bonding). Fig. 24 shows the energy absorption capacity of the bilayer

composite plate with BF and FF configurations with different interface bonding strength. It can be seen that increase bonding has negative effect on ballistic performance of composite for both BF and FF configurations. This parameter specially affects the BF configuration. It is shown that in BF configuration when there is no bonding, rubber plate can stretch without any limitation and have the best performance. By increasing the interface bonding between the rubber and aluminum plate, the energy absorption of bilayer composite decreases. It can be seen that there is a critical interface bonding point which BF and FF configurations has same performance. BF configuration has the better performance for interface bonding values less than critical point. On the other hand, by increasing the bonding beyond the critical point, the FF configuration has better performance.

Figs. 25 and 26 show the deformation of bilayer composite for BF and FF configuration, respectively. It can be seen that bonding restricts the rubber deformation and doesn't let the rubber layer to present its stretch and damping properties.

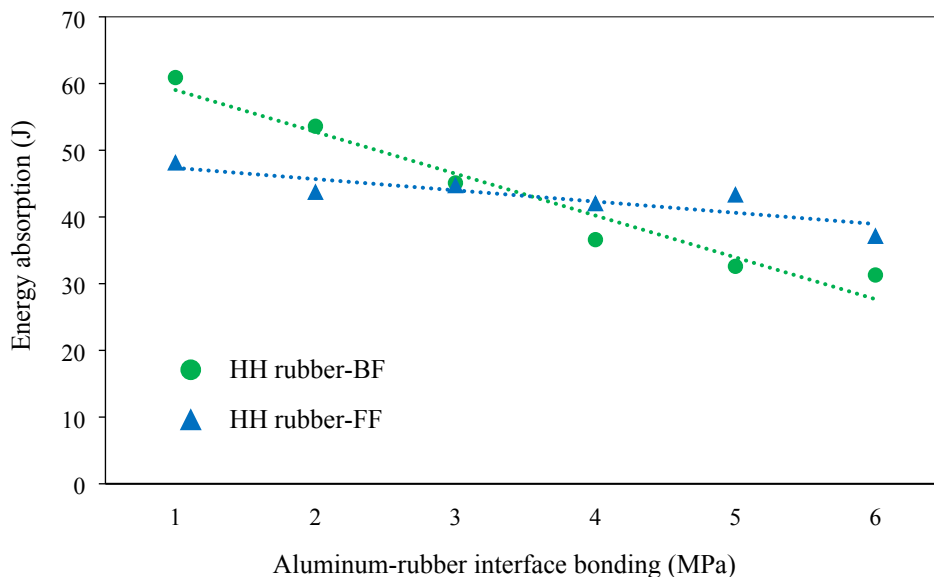


Fig. 24 Energy absorption of Al-HH rubber composite with different interface bonding for BF and FF configuration

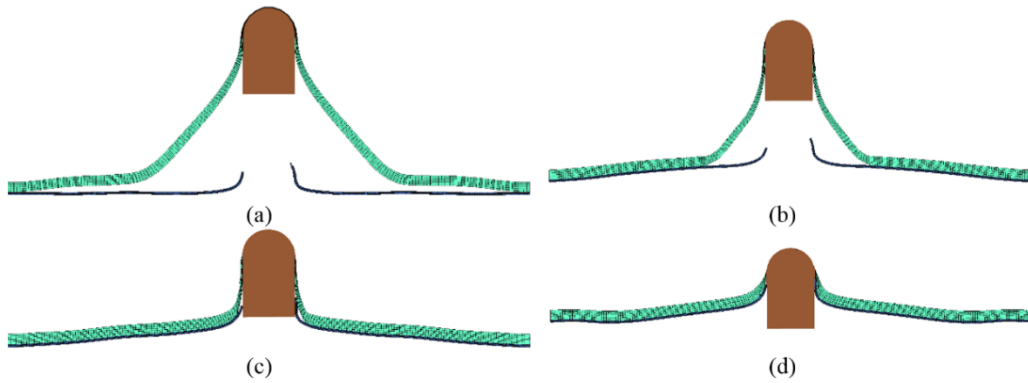


Fig. 25 Impact behavior of Al-rubber composite at initial velocity of 144 m/s for BF configuration with interface boning of (a) 0-0 (b) 20S-12N (c) 80S-50N (d) Tie

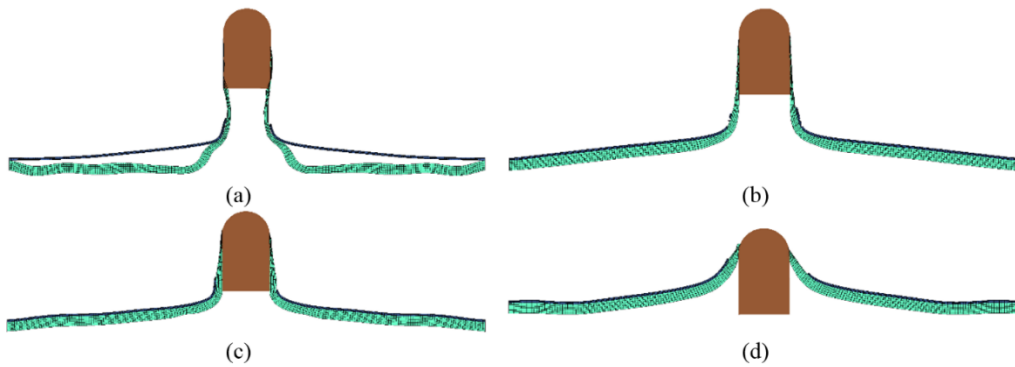


Fig. 26 Impact behavior of Al-rubber composite at initial velocity of 144 m/s for FF configuration with interface boning of (a) 0-0 (b) 20S-12N (c) 80S-50N (d) Tie

5.5. Aluminum-rubber sandwich panel

A simulation was performed to evaluate the response of an aluminum-rubber sandwich panel under impact loading. For this purpose, a 0.5 mm aluminum plate was sandwiched between two layers of HH rubber panel with thickness of 1 mm as shown in Fig. 27. The shear and normal stress at bonding interfaces were assumed to be 80 MPa and 50 MPa, respectively. Simulations were conducted at three initial velocity of projectile which were 101, 144 and 168 m/s. The residual velocity of projectile was obtained in each simulation and compared to the results of bilayer aluminum-rubber composite which presented in Table 6.

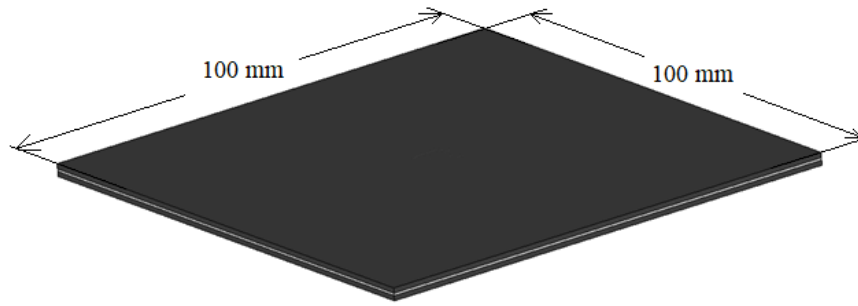


Fig. 27 Aluminum-rubber sandwich panel

It can be seen bilayer composite has better performance under impact loading compared to aluminum-rubber sandwich panel. The table shows better performance in terms of lower residual velocity for both BF and FF configuration of bilayer aluminum-rubber composite compared to aluminum-rubber sandwich panel.

Table 6 Comparison of performance of bilayer and sandwich composite

Initial velocity (m/s)		101	144	168
	Sandwich panel	75.6	125.6	152.1
Residual velocity (m/s)	Bilayer composite with BF configuration	64.5	117.2	141.5
	Bilayer composite with FF configuration	53.6	107	137.6

Perforated specimens under impact velocity of 144 m/s is shown in Fig. 28. Fig. 28 (a) and (b) show the bilayer composite in FF and BF configuration, respectively and Fig 28 (c) shows the sandwich panel response. Fig. 29 shows the aluminum plate used in specimens after perforation. It can be seen that by decreasing the rubber thickness on back face of aluminum plate, the larger petals are shown at penetration zone.

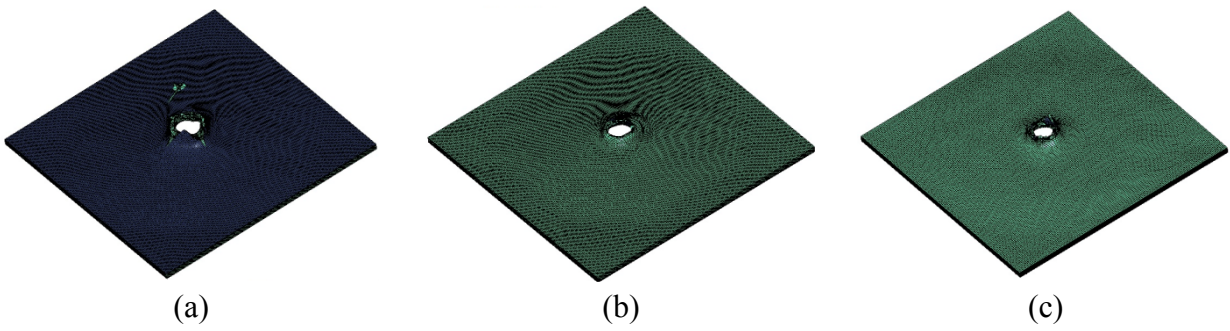


Fig. 28 Penetration of projectile in (a) Al-rubber composite with FF configuration (b) Al-rubber composite with BF configuration (c) Sandwich panel

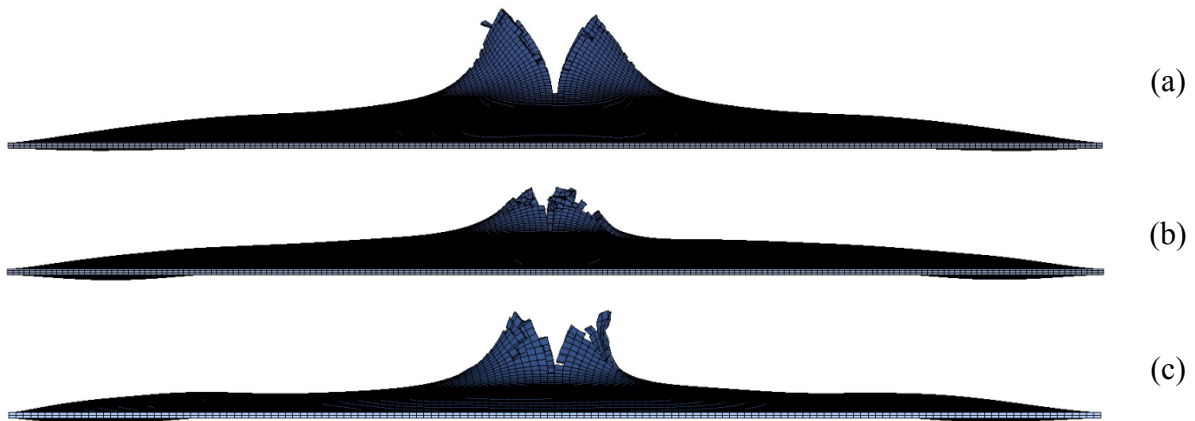


Fig. 29 Fracture of aluminum layer in (a) Al-rubber composite with FF configuration (b) Al-rubber composite with BF configuration (c) Sandwich panel

6. Conclusion

In this paper, mechanical behavior of an aluminum-rubber bilayer composite target plate under impact loading was investigated. A series of experimental tests were conducted using a gas gun at projectile velocities of 75 m/s, 101 m/s, 144 m/s and 168 m/s. From the experiments, it was focused on the ballistic performance of composite plate considering the relative position of the rubber layer with respect to the loading direction. It was found that when rubber layer located on the front face of bilayer aluminum-rubber composite, better ballistic performance can be

achieved. A numerical simulation in parallel with experimental tests was developed. The simulation was supported using a parametric study on bilayer aluminum-rubber composite. Rubber mechanical properties, as a strain rate dependent material, were obtained by SHPB tests and assigned to the model. A close agreement was found between numerical and experimental results.

Following conclusions can be highlighted from the parametric study:

1- The ballistic limits of bilayer composite with BF and FF configuration were 84.5 and 95 m/s, respectively which show 67.3% and 88.1% increase compared to the ballistic limit of the monolithic aluminum plate.

2- The ballistic performance of aluminum-rubber composite is highly dependent onto the hardness of rubber. The composite sample with higher hardness rubber can resist more efficiently against the projectile impact.

3- Increase the thickness of the rubber layer improves the overall performance of the bilayer plates for both BF and FF configurations. On the other hand, the FF configuration is more sensitive to the rubber thickness.

4- By increasing the interface bonding between the rubber and aluminum plate, the energy absorption of bilayer composite target decreases. There is a critical threshold for the interface bonding. For the case of BF configuration, the energy absorption would be higher if the bonding values are less than critical point. For the case of FF configuration, by increasing the bonding strength beyond the critical point, the ballistic performance would be higher.

References

- [1] G. Tiwari, M. Iqbal, P. Gupta, Energy absorption characteristics of thin aluminium plate against hemispherical nosed projectile impact, *Thin-Walled Structures* 126 (2018) 246-257.
- [2] Z. Rosenberg, R. Kositski, E. Dekel, On the perforation of aluminum plates by 7.62 mm APM2 projectiles, *International Journal of Impact Engineering* 97 (2016) 79-86.
- [3] M. Iqbal, S. Khan, R. Ansari, N. Gupta, Experimental and numerical studies of double-nosed projectile impact on aluminum plates, *International Journal of Impact Engineering* 54 (2013) 232-245.
- [4] M. Rodriguez-Millan, D. Garcia-Gonzalez, A. Rusinek, F. Abed, A. Arias, Perforation mechanics of 2024 aluminium protective plates subjected to impact by different nose shapes of projectiles, *Thin-Walled Structures* 123 (2018) 1-10.
- [5] K. Senthil, M. Iqbal, B. Arindam, R. Mittal, N. Gupta, Ballistic resistance of 2024 aluminium plates against hemispherical, sphere and blunt nose projectiles, *Thin-Walled Structures* 126 (2018) 94-105.
- [6] K. Ackland, C. Anderson, T.D. Ngo, Deformation of polyurea-coated steel plates under localised blast loading, *International Journal of Impact Engineering* 51 (2013) 13-22.
- [7] R. Gamache, C. Giller, G. Montella, D. Fragiadakis, C. Roland, Elastomer-metal laminate armor, *Materials & Design* 111 (2016) 362-368.
- [8] I. Mohagheghian, G.J. McShane, W. Stronge, Quasi-static and impact perforation of polymer-metal bi-layer plates by a blunt indenter, *Thin-walled structures* 117 (2017) 35-48.
- [9] M. Amini, J. Simon, S. Nemat-Nasser, Numerical modeling of effect of polyurea on response of steel plates to impulsive loads in direct pressure-pulse experiments, *Mechanics of Materials* 42(6) (2010) 615-627.
- [10] M. Amini, J. Isaacs, S. Nemat-Nasser, Investigation of effect of polyurea on response of steel plates to impulsive loads in direct pressure-pulse experiments, *Mechanics of Materials* 42(6) (2010) 628-639.
- [11] C. Roland, D. Fragiadakis, R. Gamache, Elastomer–steel laminate armor, *Composite structures* 92(5) (2010) 1059-1064.
- [12] C. Roland, D. Fragiadakis, R. Gamache, R. Casalini, Factors influencing the ballistic impact resistance of elastomer-coated metal substrates, *Philosophical Magazine* 93(5) (2013) 468-477.
- [13] M. Grujicic, B. Pandurangan, T. He, B. Cheeseman, C.-F. Yen, C. Randow, Computational investigation of impact energy absorption capability of polyurea coatings via deformation-induced glass transition, *Materials Science and Engineering: A* 527(29-30) (2010) 7741-7751.
- [14] H. Yang, X.-F. Yao, S. Wang, Y.-C. Ke, S.-H. Huang, Y.-H. Liu, Analysis and Inversion of Contact Stress for the Finite Thickness Neo-Hookean Layer, *Journal of Applied Mechanics* 85(10) (2018) 101008.
- [15] A. Khodadadi, G. Liaghat, A.R. Bahramian, H. Ahmadi, Y. Anani, S. Asemani, O. Razmkhah, High velocity impact behavior of Kevlar/rubber and Kevlar/epoxy composites: A comparative study, *Composite Structures* 216 (2019) 159-167.
- [16] H. Pouriayevali, Y. Guo, V. Shim, A visco-hyperelastic constitutive description of elastomer behaviour at high strain rates, *Procedia Engineering* 10 (2011) 2274-2279.
- [17] H. Yang, X. Yao, Z. Zheng, L. Gong, L. Yuan, Y. Yuan, Y. Liu, Highly sensitive and stretchable graphene-silicone rubber composites for strain sensing, *Composites Science and Technology* 167 (2018) 371-378.
- [18] N. Hassim, M.R. Ahmad, W.Y.W. Ahmad, A. Samsuri, M.H.M. Yahya, Puncture resistance of natural rubber latex unidirectional coated fabrics, *Journal of Industrial Textiles* 42(2) (2012) 118-131.
- [19] Y. Dong, Y. Ke, Z. Zheng, H. Yang, X. Yao, Effect of stress relaxation on sealing performance of the fabric rubber seal, *Composites Science and Technology* 151 (2017) 291-301.

- [20] H. Yang, X.-F. Yao, Y.-C. Ke, Y.-j. Ma, Y.-H. Liu, Constitutive behaviors and mechanical characterizations of fabric reinforced rubber composites, *Composite Structures* 152 (2016) 117-123.
- [21] H. Yang, X.-F. Yao, H. Yan, Y.-n. Yuan, Y.-F. Dong, Y.-H. Liu, Anisotropic hyper-viscoelastic behaviors of fabric reinforced rubber composites, *Composite Structures* 187 (2018) 116-121.
- [22] A. Khodadadi, G. Liaghat, H. Ahmadi, A.R. Bahramian, O. Razmkhah, Impact response of Kevlar/rubber composite, *Composites Science and Technology* 184 (2019) 107880.
- [23] M. Bhattacharya, A.K. Bhowmick, Synergy in carbon black-filled natural rubber nanocomposites. Part I: Mechanical, dynamic mechanical properties, and morphology, *Journal of materials science* 45(22) (2010) 6126-6138.
- [24] H.H. Cai, S.D. Li, G.R. Tian, H.B. Wang, J.H. Wang, Reinforcement of natural rubber latex film by ultrafine calcium carbonate, *Journal of applied polymer science* 87(6) (2003) 982-985.
- [25] S. Manroshan, A. Baharin, Effect of nanosized calcium carbonate on the mechanical properties of latex films, *Journal of Applied Polymer Science* 96(5) (2005) 1550-1556.
- [26] X. Li, Z. Li, Y. Xia, Test and calculation of the carbon black reinforcement effect on the hyper-elastic properties of tire rubbers, *Rubber Chemistry and Technology* 88(1) (2015) 98-116.
- [27] L. Yang, V. Shim, C. Lim, A visco-hyperelastic approach to modelling the constitutive behaviour of rubber, *International Journal of Impact Engineering* 24(6-7) (2000) 545-560.
- [28] Y. Bai, C. Liu, G. Huang, W. Li, S. Feng, A Hyper-Viscoelastic Constitutive Model for Polyurea under Uniaxial Compressive Loading, *Polymers* 8(4) (2016) 133.
- [29] L.-D.K.U.s. Manual, I. Volume, Version 971, Livermore Software Technology Corporation 7374 (2007) 354.
- [30] K. Spranghers, D. Kakogiannis, J. Ndambi, D. Lecompte, H. Sol, Deformation measurements of blast loaded plates using digital image correlation and high-speed photography, *EPJ Web of Conferences*, EDP Sciences, 2010, p. 12006.
- [31] M. Ghalami-Chooabar, M. Sadighi, Investigation of high velocity impact of cylindrical projectile on sandwich panels with fiber-metal laminates skins and polyurethane core, *Aerospace Science and Technology* 32(1) (2014) 142-152.
- [32] A. Khodadadi, G. Liaghat, H. Ahmadi, A.R. Bahramian, Y. Anani, O. Razmkhah, S. Asemeni, Numerical and experimental study of impact on hyperelastic rubber panels, *Iranian Polymer Journal* (2018) 113-122.